ELSEVIER

Materials Chemistry and Physics 71 (2001) 179–189

MATERIALS CHEMISTRY AND PHYSICS

www.elsevier.com/locate/matchemphys

Synthesis of Eu^{3+}-activated yttrium oxysulfide red phosphor by flux fusion method

Chung-Lun Lo [a], Jenq-Gong Duh [a,*], Bi-Shiou Chiou [b], Chao-Chi Peng [c], Lyuji Ozawa [c]

[a] *Department of Materials Science and Engineering, National Tsing Hua University, HsinChu, Taiwan, ROC*
[b] *Department of Electronics Engineering and Institute of Electronics, National Chiao Tung University, HsinChu, Taiwan, ROC*
[c] *Electronics Research and Service Organization, Industrial Technology Research Institute, HsinChu, Taiwan, ROC*

Received 15 June 2000; received in revised form 6 December 2000; accepted 20 December 2000

Abstract

Synthesis of the yttrium oxysulfide red phosphor by the flux fusion method was presented. Effects of flux compositions and sintering conditions on the shape and size distribution of phosphor were studied. In addition, the optimization of firing conditions was also conducted. After firing phosphor with a flux containing $(S + Na_2CO_3 + Li_3PO_4 + K_2CO_3)/(S + Li_2CO_3 + K_2CO_3)$ at a ratio of 3:1 at 1150°C for 2.5 h, $Y_2O_2S:Eu^{3+}$ phosphor was obtained without any Y_2O_3 as a second phase. The nearly spherical phosphor powder exhibited a mean particle size of 3 μm and a rather sharp particle size distribution. $Y_2O_2S:Eu^{3+}$ red phosphor illuminated the most red color light with an applied probe current density of 0.51 $\mu A/cm^2$.

Keywords: Phosphor; Yttrium oxysulfide; Flux fusion; Cathodoluminescence

1. Introduction

Phosphor is defined as material that emits photons with high luminescence efficiency. The cathodoluminescent phosphors convert electron energy into visible light and are used in the display devices as the screen material. Trivalent rare-earth ions have usually been selected to be used as activators in line-emitting phosphors because the spectral emission lines of trivalent rare-earth ions in the host lattice are rather narrow [1,2]. Yttrium oxysulfide doped with europium ($Y_2O_2S:Eu^{3+}$) red phosphor is a high efficiency cathodoluminescent material that is used extensively in the phosphor screen of display devices. $Y_2O_2S:Eu^{3+}$ has the sharper emission lines leading to better colorimetric definition and higher luminescence efficiency than the other red phosphors [3,4].

The fabrication of good $Y_2O_2S:Eu^{3+}$ red phosphor is not an easy task. There are several methods known: (i) reduction of rare-earth sulfate by H_2 or CO [5,6]; (ii) sulfuration of rare-earth oxide by H_2S or CS_2 [7]; (iii) reaction between an oxide and a sulfide [8]; (iv) sulfuration of rare-earth oxide in the atmosphere of $N_2 + H_2O + H_2S$ [9] and (v) sulfuration of rare-earth oxide in the flux [10–15]. Among all the synthesis methods, the sulfuration of a mixture of yttrium and europium oxides in the flux is the most important since it is mass producible. A flux is a material that melts lower than the solid-state reaction temperature, dissolves one or more of the components and allows material transport to the reaction zone, without entering into the solid-state reaction. Preferably, the end-product should be insoluble in the flux. The flux materials usually include Na_2O_3, K_2CO_3, K_3PO_4, etc. [16–20].

The shape and size of phosphor particles are critical in the fabrication of high quality displayers. Phosphor used in both CRT and X-ray screen with uniform size distribution (3–7 μm) of the particles results in the best screen surfaces [21]. Reducing the particle size gives a higher resolution [22–24]. Optimizing the particle size distribution will lead to a higher packing density for phosphor layers, and thus to a higher resolution, too. Spherical particles also give a high packing density and the small light-scattering coefficient [25,26]. Thus, the sphere-like phosphor powder is required.

The fabrication of $Y_2O_2S:Eu^{3+}$ phosphor by flux fusion method was first proposed by one of the authors, Ozawa [10,27]. Recently, a preliminary study on spectral properties of Eu^{3+}-activated yttrium oxysulfide red phosphor was report [28]. In the present study, sphere-like $Y_2O_2S:Eu^{3+}$ phosphor was fabricated by flux fusion method. The effects of various flux compositions on the powder shape and size distribution were investigated. In addition, the cathodolu-

* Corresponding author. Tel.: +886-3-5712686; fax: +886-3-5712686.
E-mail address: jgd@mse.nthu.edu.tw (J.-G. Duh).

0254-0584/01/$ – see front matter
PII: S0254-0584(01)00279-6

Table 1
Composition of starting materials for phosphors

Materials	wt.%	Remark
Phosphors with flux A		
Y_2O_3	46.73	Host materials
Eu_2O_3	2.80	Activator
S	22.43	Host materials
Na_2CO_3	16.35	Base materials of flux
Li_3PO_4	9.35	Flux for round particles
K_2CO_3	2.34	Softening rods
Phosphors with flux B		
Y_2O_3	49.80	
Eu_2O_3	2.98	
S	21.94	
K_2CO_3	2.49	
Li_2CO_3	22.79	

minescence properties of the as-fabricated $Y_2O_2S:Eu^{3+}$ phosphor would be presented and discussed.

2. Experimental procedures

Europium-doped yttrium oxysulfide was prepared by sulfide-fusion method. The raw materials of Y_2O_3 and Eu_2O_3 were mixed with different compositions of flux, containing S, Na_2CO_3, K_2CO_3, Li_2CO_3 and Li_3PO_4. Two different flux noted as A and B are listed in Table 1, and the designation of test samples is shown in Table 2.

The raw materials were fired at temperatures in the range of 1000–1200°C to undergo a solid-melt reaction between the rare-earth oxides and Na_2S_x polysufide. The overall reaction for the forming process of red phosphor, $Y_2O_2S:Eu^{3+}$, can be represented as

$$\begin{aligned} &Y_2O_3 + Eu_2O_3 + \text{flux}\ (S + Na_2CO_3 + \cdots) \\ &\quad \rightarrow Y_2O_2S:Eu^{3+} + \text{flux residue}\ (Na_2S_x + Na_2SO_4) \\ &\qquad + \text{gaseous products}\ (HS + SO_4 + CO_2 + O) \end{aligned} \quad (1)$$

The atmosphere in the heating tube was controlled to be oxygen-free during firing. The as-fabricated phosphor powder was examined with a scanning electron microscope (SEM, JEOL 840A, Japan) to investigate the particle size, particle shape and surface morphology. The phosphor powder was further examined with a Laser Particle Sizer (Analysette 22, Fritsch) to evaluate the particles size distribution.

The phase and crystal structure of the as-fabricated phosphor were identified by means of a X-ray diffractometer (D/MAX-B, Rigaku, Japan) with a wavelength of Cu Kα ($\lambda = 1.5406$ Å). The scanning rate was 20/min.

In the luminescence measurement system, the electron probe was generated and accelerated by the electron gun, and focused on the phosphor sample with a certain spot size. The cathodoluminescence spectrum of phosphors was measured with a Fourier transform analysis instruments, and the CIE (Commission Internationale de l'Eclairage) color coordinates of phosphor were examined with a colormeter (Minolta CS-100, Japan).

3. Results and discussion

3.1. Synthesis of phosphor powders

$Y_2O_2S:Eu^{3+}$ red phosphors were prepared by the flux fusion method, by heating a mixture of Y_2O_3, Eu_2O_3 and flux to various temperatures ranged from 1000 to 1200°C for different firing times. Fig. 1 shows XRD spectra of phosphors using flux A after firing between 1000 and 1200°C for 2.5 h. The phosphor samples fired at either 1000 or 1100°C exhibit peaks corresponding to the Y_2O_3 phase, as illustrated in Fig. 1a and b. The XRD lines observed in samples fired at 1150°C (Fig. 1c) and 1200°C (Fig. 1d) matched those of Y_2O_2S structure given in standard JCPDS files [29]. This indicates that the starting phosphor materials with flux A sintered at the temperature below 1100°C fail to completely convert into the Y_2O_2S phase and thus there is residual Y_2O_3 left. It is concluded that the firing temperature should be above 1100°C for phosphor firing with flux A. However, for starting phosphor materials with flux B (containing Li_2CO_3), the sample fired at 1150°C for 4 h exhibits almost fully Y_2O_2S without the presence of the Y_2O_3 phase.

In fact, firing time is also an important parameter, which has a critical effect on the final product. The firing conditions of phosphors are different for various flux compositions. X-ray analysis gives the evidence that it is necessary for samples with flux B to be fired at 1150°C for 4 h to efficiently obtain Y_2O_2S phosphor host materials. However, for

Table 2
Designation of test samples

Flux	Firing temperature (°C)		
	1100	1150	1200
Pure flux A	1100A	1150A	1200A
Pure flux B	1100B	1150B	1200B
Mixture with flux A:flux B = 1:1	1100A1B1	1150A1B1	1200A1B1
Mixture with flux A:flux B = 2:1	1100A2B1	1150A2B1	1200A2B1
Mixture with flux A:flux B = 3:1	1100A3B	1150A3B	1200A3B1
Mixture with flux A:flux B = 1:2	1100A1B2	1150A1B2	1200A1B2

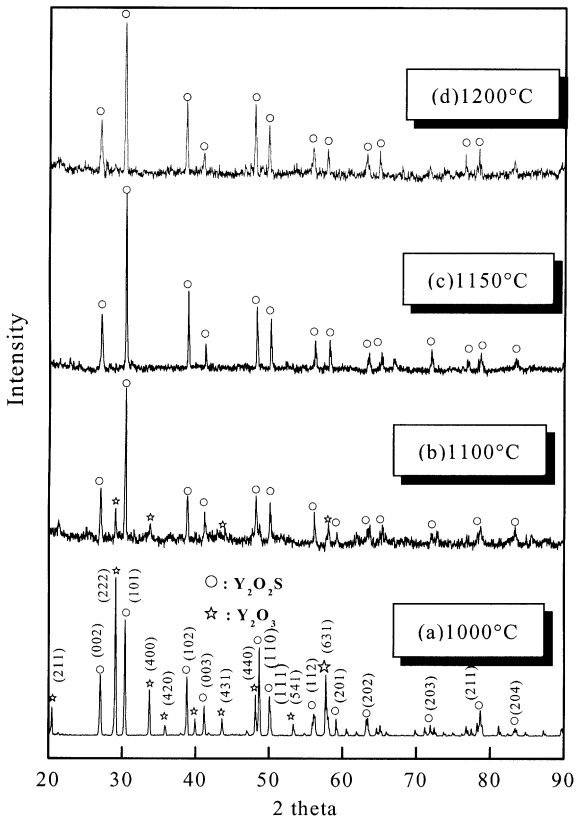

Fig. 1. X-ray diffraction patterns of the phosphor containing flux A after firing for 2.5 h at various temperatures: (a) 1000°C; (b) 1100°C; (c) 1150°C; (d) 1200°C.

samples with flux A, the starting materials are totally converted into Y_2O_2S at 1150°C for less than 1 h. In addition, X-ray analysis reveals that for samples with the mixture of flux A and B fired above 1100°C, Y_2O_2S phosphors can be obtained without Y_2O_3 remained.

X-ray diffraction analysis also demonstrates that the $Y_2O_2S{:}Eu^{3+}$ is a hexagonal crystal structure with unit cell dimensions $a = 0.381$ nm and $c = 0.659$ nm. This is in agreement with the ASTM index file for Y_2O_2S of $3D^3_{3d}$ (*P3m*) space group [30,31], in which the point of symmetry of yttrium site is C_{3v} (*3m*). The trivalent europium ion is expected to occupy the yttrium site in $Y_2O_2S{:}Eu^{3+}$ since the ionic radius of Eu^{3+} (0.112 nm) is slightly larger than that of Y^{3+} (0.106 nm). Thus, Eu^{3+} substitutes Y^{3+} without disturbing the crystal lattice.

3.2. Characterization of phosphor powder

For the $Y_2O_2S{:}Eu^{3+}$ phosphor fabricated by flux method, the crystal nucleation and growth is associated with the flux at high temperature. Not only the firing conditions, such as firing temperature and firing time, but also the flux status would affect the growth of $Y_2O_2S{:}Eu^{3+}$ particles. Ozawa once reported the growth mechanism of $Y_2O_2S{:}Eu^{3+}$ microcrystallines [25]. By the particle growth model, the rate of the particle growth ($d\phi/dt$) in the presence of a flux can be given as follows:

$$\frac{d\phi}{dt} = A \exp\left(\frac{-\Delta E}{kT}\right) \tag{2}$$

where A is a constant for a given flux and crystal, t the time, k the Boltzmann constant, T the temperature in K, and ΔE is the activation energy which is given by a combination of Gibbs' free energy on the crystal surface and activation energy of diffusion for Y_2O_2S in the flux. It is assumed that for the nuclei in the mixed oxide system in the molten flux, an identical interface structure for the nucleation can be expected [32]. The activation energy is written as

$$\Delta E = N(G_v + \sigma)\lambda, \quad \Delta E \cong N\sigma\lambda \tag{3}$$

This implies that the change in free energy is a direct function of the product of the number of nuclei, N (crystallite); surface energy, σ (the surface area), and the volume of nuclei, λ. In Kottaisamy's study [33], the additional compound such as K_3PO_4 would increase the surface energy term in a linear fashion with the concentration of K_3PO_4 flux. In this study, It is argued that the additional compound, such as Li_3PO_4 in flux A, plays the same role. Thus, the increased

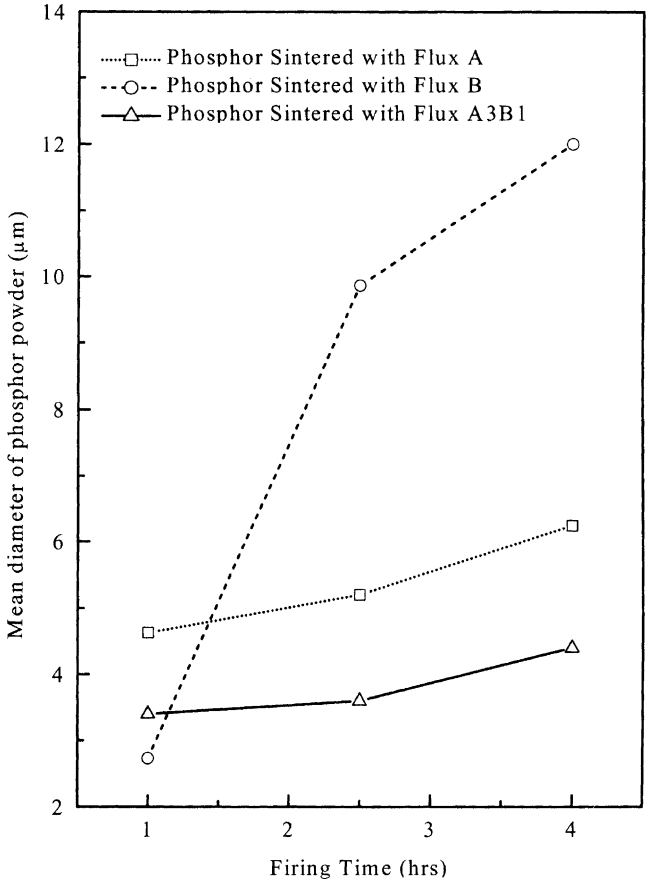

Fig. 2. Dependence of mean particle size on firing time for samples fired with different kinds of flux at 1150°C.

surface energy is expected to slow down the particle growth rate from Eq. (2).

To discuss the effects of flux compositions on the growth of $Y_2O_2S:Eu^{3+}$ particle, the relationship between particle size and flux is illustrated in Figs. 2 and 3. For Y_2O_2S phosphor fired at 1150°C for 1–4 h, as shown in Fig. 2, the particle growth rate using flux A (contained Li_3PO_4) is smaller than that using flux B (without containing Li_3PO_4). Accordingly, with the mixture of flux A and B for phosphor firing, the particle growth rate and the particle size can be reduced. Fig. 3 shows the relationship between particle size and firing temperature for $Y_2O_2S:Eu^{3+}$ phosphors fired with different flux compositions for 2.5 h. In Fig. 3, it is apparent that the mean particle size of phosphor using flux B is larger than that using either flux A or A3B1. In fact, the addition of Li_3PO_4 helps to minimize the mean diameter of the phosphor product.

The constituent Li_2CO_3 in flux B is observed to reduce the initial particle size, i.e. nucleus of Y_2O_2S phosphor crystal. The initial mean particle size fired at 1150°C for 1 h is estimated about 2.8 μm (see Fig. 2), which is smaller than the Y_2O_3 raw material around 5 μm. It is argued that the dissolution of Y_2O_3 particle in the flux takes place. It is also expected that the Li_2CO_3 in the flux solution enhances the ability for dissolving Y_2O_3 particle. The initial particle size in flux A containing Na_2CO_3 fired at 1150°C for 1 h is about 4.7 μm which is slightly smaller than the Y_2O_3 raw material (5 μm). It is reported that the dissolution of a particle of Y_2O_3 which is the seed crystal for Y_2O_2S crystal nucleation and growth is restricted in a small domain of the flux solution just covering on particle [10]. This means that the particle size distribution of the raw material Y_2O_3 is reproduced in the staring particle of Y_2O_2S growth. Fig. 4 is the particle size distribution (PSD) diagram of samples fired with flux A, B, A2B1 and A3B1, respectively, at 1150°C for 2.5 h. The sample using flux A3B1 exhibits the narrowest distribution with particle size ranging from 2 to 7 μm without agglomeration or aggregation.

Shapes of the particle are apparently different by using different compositions in flux. From SEM photographs (as shown in Fig. 5), the $Y_2O_2S:Eu^{3+}$ phosphor using flux A fired at both 1150 and 1200°C exhibits smooth, well formed polycrystalline particles, although partial particle agglomeration or aggregation is observed.

For samples fired with flux B, they all exhibit the similar shape, having strong orientation during grain growth. This means that those particles surrounded with flux B grow

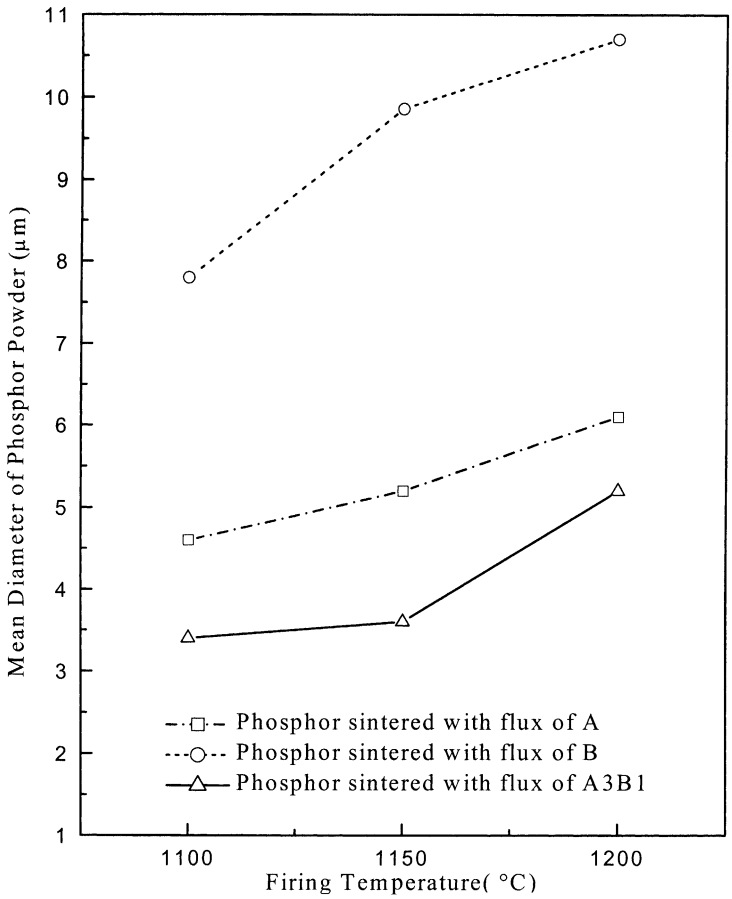

Fig. 3. Dependence of mean particle size on firing temperature for samples fired with different kinds of flux for 2.5 h.

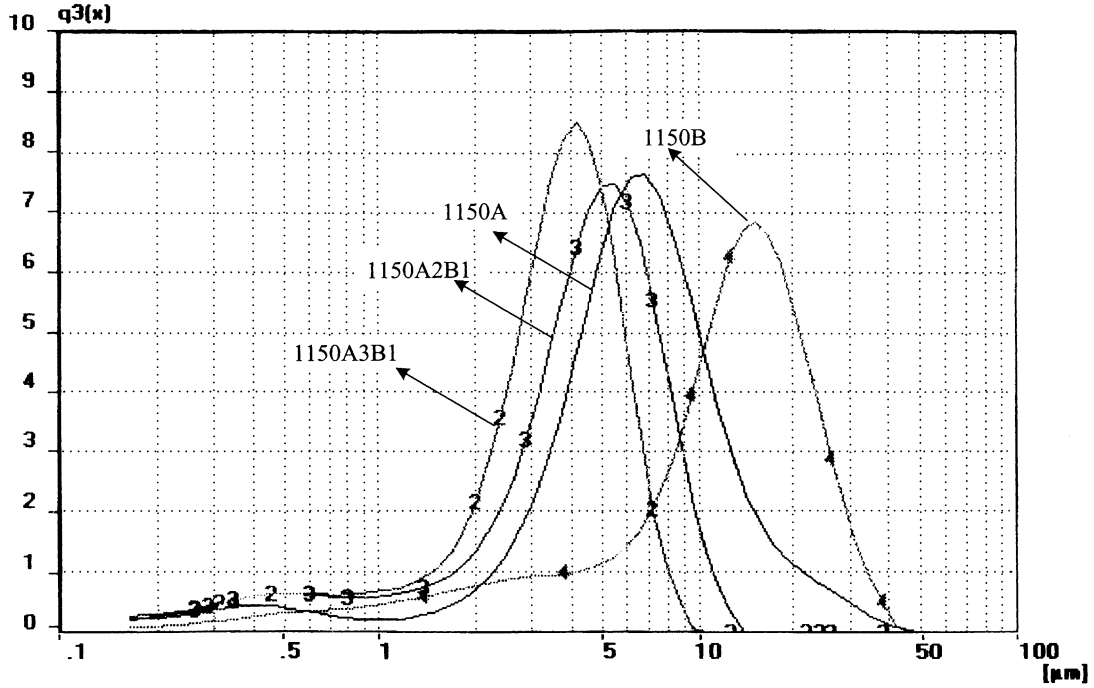

Fig. 4. Particle size distribution diagram of samples fired with flux A, B, A2B1 and A3B1 at 1150°C for 2.5 h.

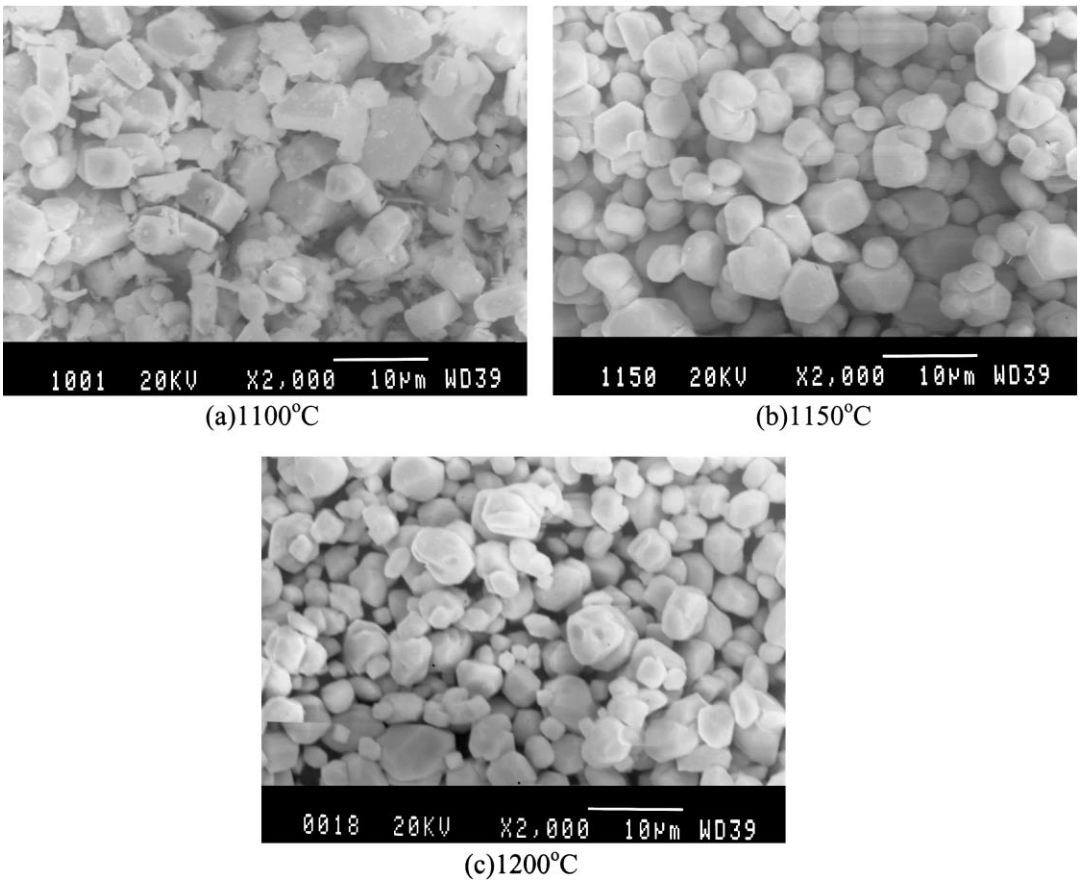

Fig. 5. SEM micrographs for samples fired with flux A for 2.5 h at various temperatures: (a) 1100°C; (b) 1150°C; (c) 1200°C.

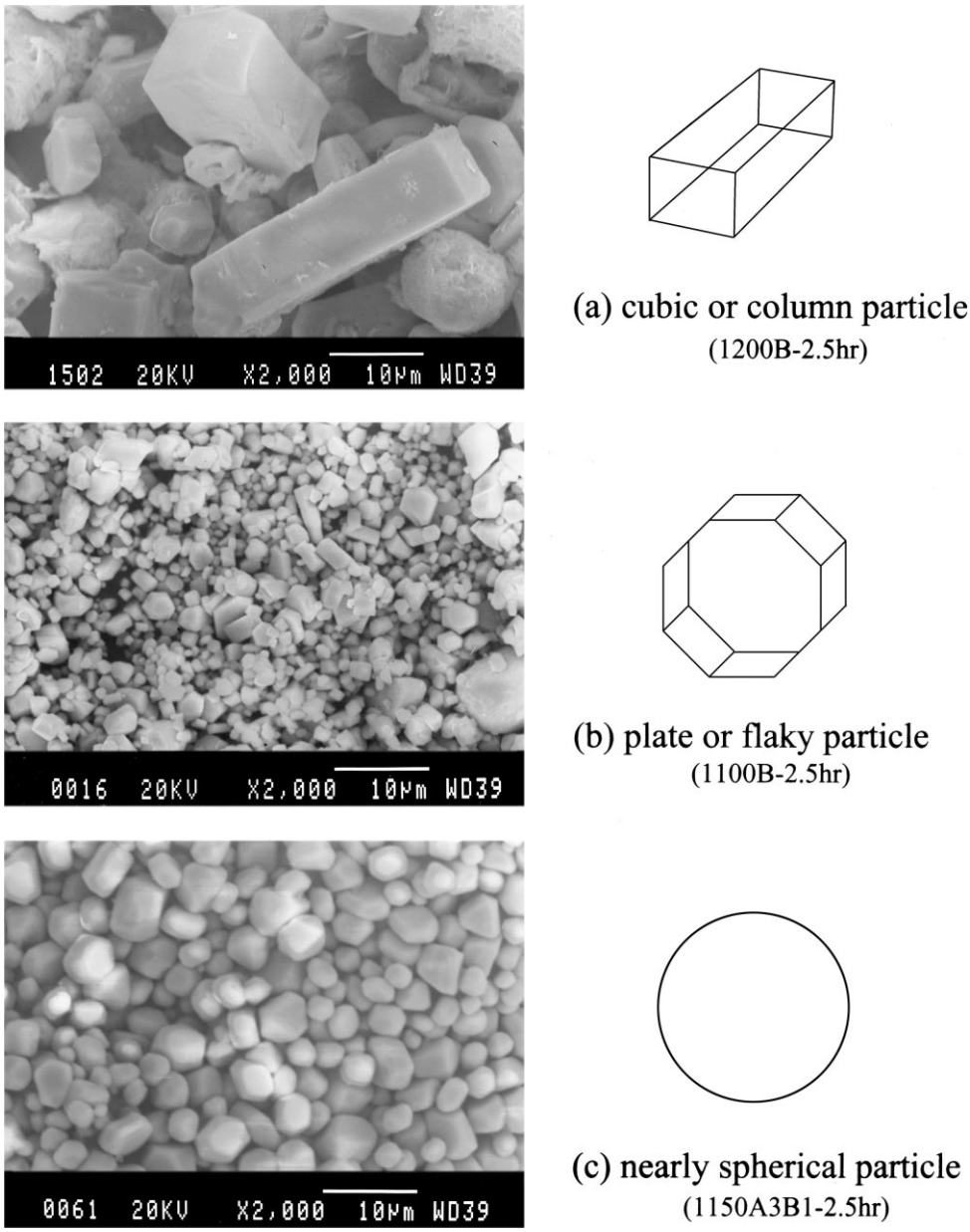

Fig. 6. Shape morphologies of fired phosphor particles: (a) cubic or column; (b) plate; (c) nearly spherical.

with a predominated orientation. Some of the solid-flux interfaces move more easily than others and interfacial free energy between these interfaces is varied [34]. The equilibrium shape is a polyhedron with the largest facets having the lowest interfacial free energy. Consequently, the forming shape of the phosphor sintered with flux B is usually flaky and hexagonal crystalline, as shown in Fig. 6a and b. However, phosphors fired with mixture flux of A3B1 tend to form sphere-like particles, as shown in Fig. 6c.

It should be pointed out that the sample preparation for PSD measurement is critical. For sample fired with flux A at 1150°C after dispersing by ultrasonic vibration, the mean diameter from PSD measurement is 11.7 μm. On the other hand, the mean particle diameter measured from SEM micrograph is about 5.6 μm. This discrepancy implies that the powder fired with flux A exhibits some degree of agglomerates. It is revealed from SEM results that the agglomerated phosphor powder in sample fired with flux A is always observed whatever the firing temperature or firing time is varied. However, in samples with other flux composition, such as flux B only or mixture of flux A and B, the agglomeration is diminished.

In consideration of the different characteristics of flux A and B, it is expected to obtain a phosphor powder with spherical shape, controlled size, and narrower distribution in particle size by mixing flux A and B. Among all samples with different firing conditions as discussed, the one with flux A3B1 is the most favorable for further application in

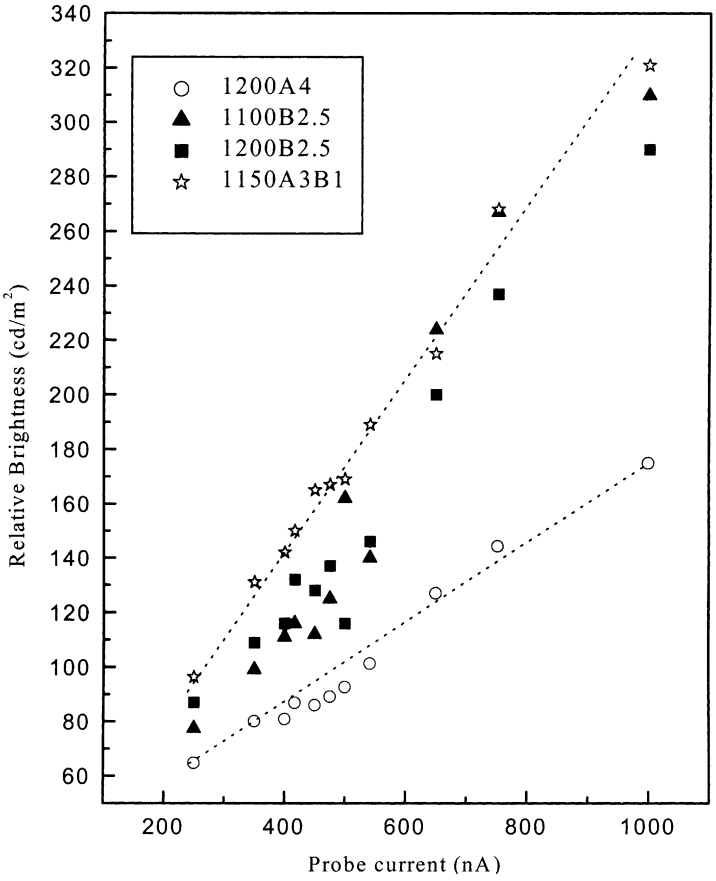

Fig. 7. Relative brightness curve for phosphor powder with different shape morphology as a function of probe current.

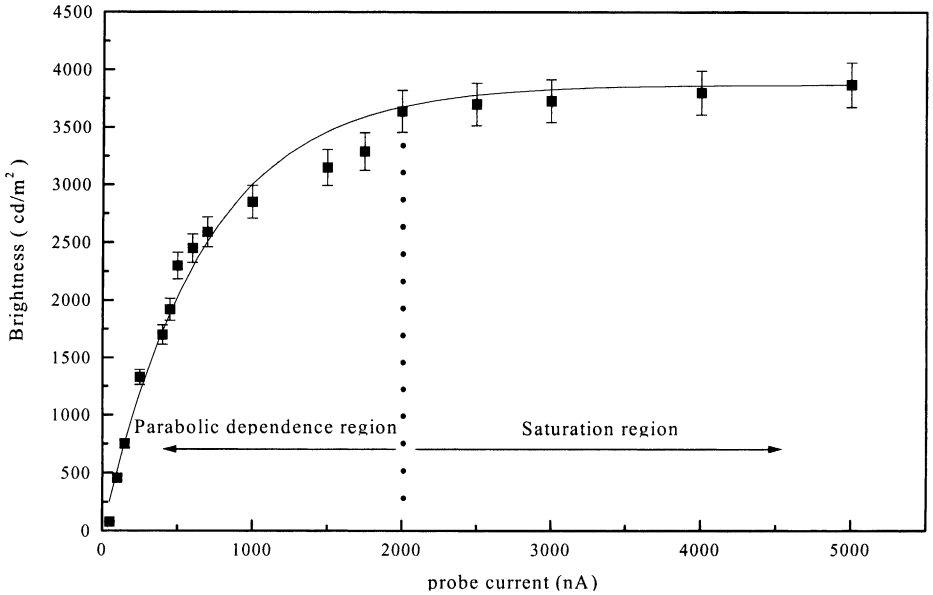

Fig. 8. Relationship between brightness and the applied probe current on phosphor.

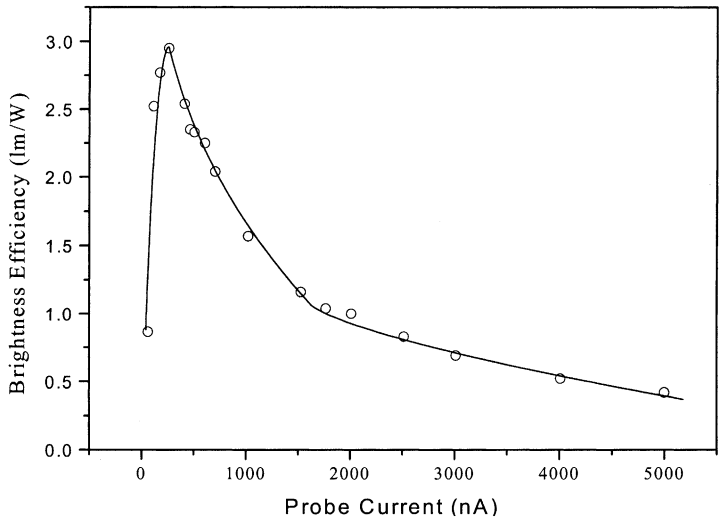

Fig. 9. Dependence of luminescence brightness efficiency on the applied probe current.

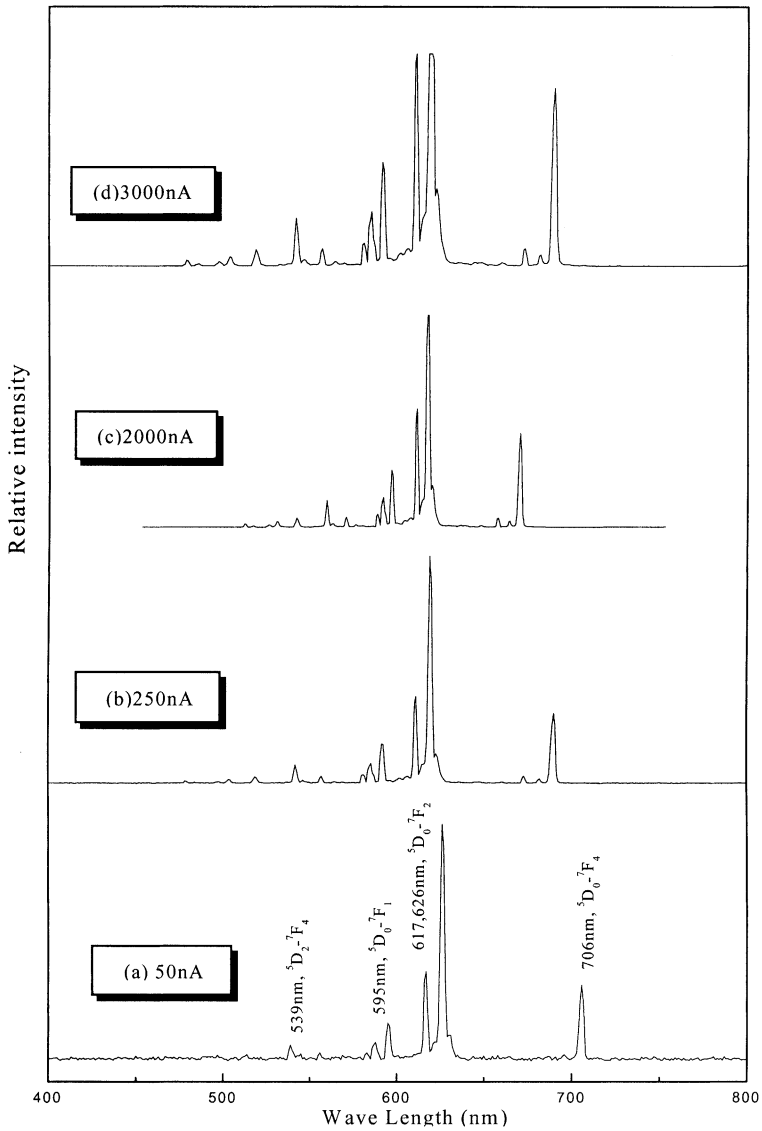

Fig. 10. Cathodoluminescence spectrum for phosphor under various probe currents: (a) 50 nA; (b) 250 nA; (c) 2000 nA, and (d) 3000 nA.

the phosphor screen due to the sphere-like shape and well dispersion of powders.

3.3. Cathodoluminescence properties of $Y_2O_2S:Eu^{3+}$

It has been discussed that phosphor powders of different shape and size can be obtained either with controlled fired condition or with various flux compositions. The shapes of phosphor particles can be divided into three category: (i) cubic or column, (ii) plate, and (iii) nearly spherical particles with smooth and flat surface. In this study, the sample 1150A4 (6.5 μm) is nearly round, while the sample 1150B2.5 (9.5 μm) is column or cubic, and the sample 1150A3B1 is smaller particle (3.3 μm) with spherical shape.

Physically speaking, particles of different shape might equally emit brilliant cathodoluminescence under electron irradiation. Nevertheless, the shape of particles would affect the emitting light in the case of phosphor screen (transmission lightness) due to various particles surface facet. In the phosphor screen, the luminescence light passes through the phosphor layers and ITO glass to the detector. The round particles emit cathodoluminescence light uniformly in all possible directions, indicating that the cathodoluminescence generated in the particles comes out from random scattering inside the particles. However, in the case of plate or flaky particles, the intensities from the basal plane of the plate particles are rather weak, while strong intensities come out from the edge of plane particles. This shape effect for phosphor screen might be attributed to the brightness curve difference in Fig. 7. The phosphor particles with the nearly round shape, such as samples of 1200A4 and 1150A3B1, exhibit a linear increase of brightness with the applied probe current. However, for the other samples containing the column and plate shape particles, such as 1100B2.5 and 1200B2.5, there is scattered data in the brightness with respect to the probe current. In the phosphor screen, each particle arranged on the first layer on the gun side emits completely scattered cathodoluminescence light, and the emitted light is further scattered by the surface of the particles situated between the emitting phosphor particles and ITO glass substrate. Thus, completely scattered cathodoluminescence light is emitted from the screen. If the light is not scattered randomly, the anisotropical intensity is detected, such as the case of light scattered in cubic, column or plate particles. The anisotropical light reflects the scattered data in the measurement of brightness as shown in Fig. 7 for samples 1100B2.5 and 1200B2.5.

The cathodoluminescent brightness was measured with the $Y_2O_2S:Eu^{3+}$ (5 wt.%) red phosphor at a constant accelerating voltage (10 kV) with various probe currents, as shown in Fig. 8. It is observed that the cathodoluminescent brightness of phosphors is saturated under the high probe current density. Before the saturation of brightness occurs, the relationship between brightness and probe current is parabolic dependence. It is thought that the total amounts of activator centers remain constant in a restricted area of spot, as the current density exceeds the limit that activator centers are required, the luminescence source is exhausted under the high energy density, and a near saturated region is achieved, as indicated in the right portion of the curve in Fig. 8.

To appreciate the energy transformation, the dependence curve of luminescence brightness efficiency (lm/W) as a function of the probe current is shown in Fig. 9. It

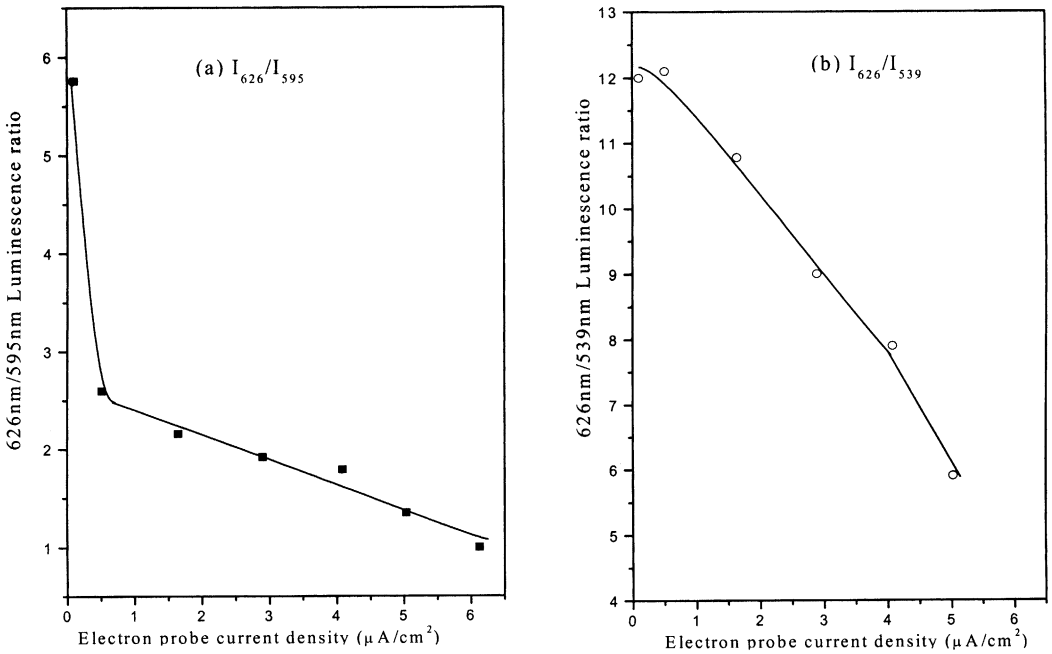

Fig. 11. Luminescence ratio as a function of the applied probe current density: (a) I_{626}/I_{595}; (b) I_{626}/I_{539}.

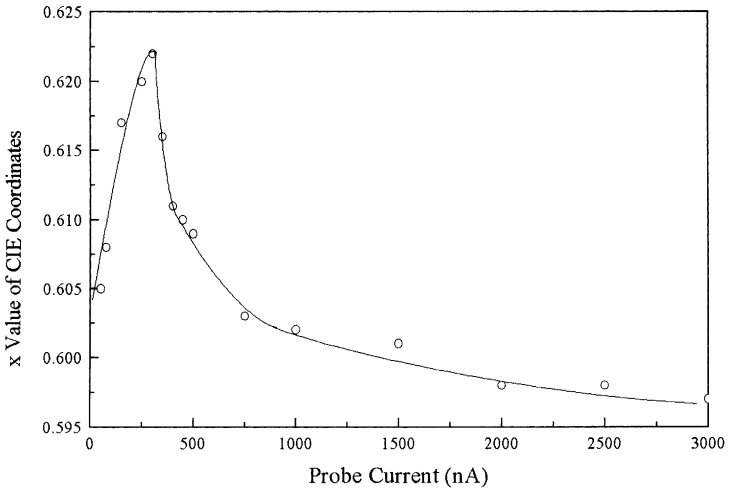

Fig. 12. The x-value of CIE coordinates as a function of the electron probe current.

appears that the maximum brightness efficiency at 3 lm/W of the phosphor sample is obtained at a probe current of 250 nA, corresponding to the electron probe current density of 0.51 μA/cm^2.

Emission spectra of Eu^{3+}-doped oxysulfide obtained at room temperature are shown in Fig. 10. The main signals are observed in the range between 580 and 630 nm, which is in agreement with the results reported by Kader and Elkholy [35]. On the basis of known energy levels of the Eu^{3+} ions and crystal field splitting in Y_2O_2S:Eu^{3+} crystals [30,31], the strongest red-emission lines at 626 and 617 nm correspond to the transition from $^5D_0$ to $^7D_2$ level. The most important line at 626 nm is the strongest emission line for the red color. Fig. 11a and b shows the dependence of the luminescence intensity ratio of both 626:595 nm (I_{626}/I_{595}) and 626:539 nm (I_{626}/I_{539}) on the applied probe current density. It indicates that the relative intensities of wavelength among 626, 659 and 539 nm vary with electron probe current, which render cathodoluminescence color shift by modifying probe current density. The fact that the relative intensity of wavelengths of 539 nm ($^5D_2$ to $^7D_4$) and 595 nm ($^5D_0$ to $^7D_1$) increases with the electron probe current means that the luminescent color changes from red to orange with increasing applied electron probe current density. It is also observed that x-coordinates of CIE chromaticity diagram shift with the increase in the electron probe current, as shown in Fig. 12. From the color sites in CIE chromaticity diagram [36,37], when $x > 0.615$, the color is red in viewing, while for $x < 0.615$, it is reddish orange. In fact, the maximum value of $I_{626\,nm}/I_{595\,nm}$ or $I_{626\,nm}/I_{539\,nm}$ around 250 nA (0.51 μA/cm^2) corresponds to the most distinct red color (CIE coordinates: $x = 0.644$, $y = 0.344$) in viewing.

4. Summary

1. Y_2O_2S phosphors doped with Eu^{3+} are fabricated by flux method. It is necessary for phosphors with flux B ($Li_2CO_3 + Na_2CO_3$) to be sintered at 1150°C for 4 h to efficiently obtain Y_2O_2S host materials. For phosphors sintered with flux A ($K_2CO_3 + Na_2CO_3 + Li_3PO_4$), the starting materials can be completely converted to Y_2O_2S at 1150°C for less than 1 h.
2. By mixing flux A with flux B at a weight ratio of 3:1, the final product is the phosphor with an average particle size of 3 μm. Narrow distribution of particles and nearly spherical particle are achieved without agglomerates by sintering at 1150°C for 2.5 h.
3. The as-fabricated Y_2O_2S:Eu^{3+} (5 wt.%) red phosphor illuminates the most red color light with an applied electron probe current density of 0.51 μA/cm^2 (10 kV) and the luminescence brightness efficiency is 3 lm/W. If more energy is applied by increasing the probe current density, the phosphor exhibits saturation of brightness and results in the color shifting from red to reddish orange.

Acknowledgements

This work is supported by the Electronics Research and Service Organization, Industrial Technology Research Institute (ERSO, ITRI), Taiwan under contract No. E87018. Partial support from National Science Council, Taiwan under the contract No NSC-89-2216-E004-041 is acknowledged.

References

[1] D.M. Yost, Tr. Russel, C.S. Garner, The Rare Earth Elements and their Compounds, Wiley, New York, 1950.
[2] K.N.R. Taylor, M.I. Darby, Physics of Rare Earth Solids, Chapman & Hall, London, 1965.
[3] M.R. Royce, U.S. Patent 3,418,245 (1968).
[4] P.N. Yocom, U.S. Patent 3,418,247 (1968).
[5] J.J. Pitha, A.L. Smith, R. Ward, J. Am. Chem. Soc. 69 (1947) 1870.
[6] M. Koskenlinna, M. Leskela, L. Niinisto, J. Electrochem. Soc.: Solid State Sci. Technol. 123 (1976) 75.

[7] J.W. Haynes, J.J. Brown, J. Electrochem. Soc.: Solid State Sci. Technol. 115 (1968) 115.
[8] D.W. Ormond, E. Blanks, J. Electrochem. Soc.: Solid State Sci. Technol. 122 (1975) 152.
[9] P. Khodadad, T. Tek, J. Flauhaut, L. Domange, Acad. Sci. 260 (1965) 2235.
[10] L. Ozawa, J. Electrochem. Soc. 124 (1977) 413.
[11] O. Kanehisa, T. Kano, H. Yomamoto, J. Electrochem. Soc.: Solid State Sci. Technol. 132 (1985) 2023.
[12] R.P. Rao, J. Electrochem. Soc. 143 (1) (1996) 189.
[13] J. Flahut, E. Attal, Compt. Rend. 238 (1954) 682.
[14] M. Picon, M. Patrie, Compt. Rend. 242 (1956) 516.
[15] L. Domange, J. Flahaut, M. Guittard, Compt. Rend. 249 (1959) 697.
[16] H.A. Eick, J. Am. Chem. Soc. 80 (1958) 43.
[17] A. Morell, J. Electrochem. Soc. 138 (14) (1991) 1100.
[18] M. Kottaisamy, R. Jagannathan, J. Electrochem. Soc. 142 (9) (1995) 3205.
[19] S.R. Mho, Korean Chem. Soc. 11 (5) (1996) 386.
[20] S.Y. Chang, Q.W. Choi, H. Choi, S.I. Mho, J. Solid State Inorg. Chem. 133 (1996) 1123.
[21] L.H. Brixner, Mater. Chem. Phys. 16 (1987) 253.
[22] K. Ohno, T. Abe, J. Electrochem. Soc. 141 (5) (1994) 1252.
[23] K. Urabe, Jpn. J. Appl. Phys. 19 (5) (1980) 885.
[24] K. Urabe, Jpn. J. Appl. Phys. 20 (1) (1981) 28.
[25] Y. Uehara, K. Nakayama, T. Asano, H. Matsukiyo, in: Proceedings of the Extended Abstracts of the 186th ECS Meeting, Vol. 94-2, 1994, p. 875.
[26] Japanese Patent Disclosure 4-45192 (1992).
[27] L. Ozawa, H.N. Hersh, J. Electrochem. Soc.: Solid-State Sci. Technol. 132 (1974) 895.
[28] Y.H. Tseng, B.S. Chiou, C.C. Peng, L. Ozawa, Thin Solid Films 330 (1998) 73.
[29] JCPDS 24-1424, Raw Data Obtained from Downey, GTE Laboratories Incorporated, Bayside, New York, USA, 1971.
[30] O.J. Sovers, T. Yoshioka, J. Chem. Phys. 49 (11) (1968) 4945.
[31] G.S. Oflet, J. Chem. Phys. 38 (1963) 2171.
[32] R.C. Ropp, Studies in Inorganic Chemistry: Luminescence and Solid State, Elsevier, Dordrecht, 1991.
[33] M. Kottaisamy, R. Jagammathan, P. Rao, M. Avudaithai, L.K. Srinivasan, V. Sundaram, J. Electrochem. Soc.: Solid State Sci. Technol. 142 (9) (1995) 3205.
[34] J.W. Christian, The Theory of Transformations in Metals and Alloys, 2nd Edition, Part I, Pergamon Press, Oxford, 1975, p. 153.
[35] A.A. Kader, M.M. Elkholy, J. Mater. Sci. 27 (1992) 2887.
[36] D.B. Judd, G. Wyszecki, Color in Business, Science, and Industry, 3rd Edition, Wiley, New York, 1975.
[37] Wyszecki, W.S. Styles, Color Science: Concepts and Methods, Quantitative Data and Formulae, 2nd Edition, Wiley, New York, 1982.